Turkish Journal of Earth Sciences (Turkish J. Earth Sci.), **Vol. 15**, 2006, pp. 95-110. *Copyright ©TÜBİTAK*

Mohr-Circle-Based Rotational Invariants of a Magnetotelluric Data Set from the Thrace Region of Turkey: Geological Implications

MURAT BAYRAK[1], AYSAN GÜRER[1], Ö. FEYZİ GÜRER[2],
O. METIN İLKIŞIK[3] & AHMET T. BAŞOKUR[4]

[1] İstanbul University, Department of Geophysical Engineering, TR–34320 İstanbul, Turkey
(E-mail: mbayrak@istanbul.edu.tr)
[2] Kocaeli University, Department of Geological Engineering, TR–41300 Kocaeli, Turkey
[3] Anadolu Yerbilimleri, Perpa-A, Şişli, TR–34385 İstanbul, Turkey
[4] Ankara University, Department of Geophysical Engineering, TR–06100 Ankara, Turkey

Abstract: In the summer of 1995, magnetotelluric data were acquired at forty sites along a southwest–northeast profile crossing northwestern Turkey in continental Europe. The traverse, 204 km in length, crossed the boundary between a metamorphic mass called the Istranca Massif and a large Tertiary sedimentary basin called the Thrace Basin. The pseudosections of Mohr-circle-based rotational invariant characteristics of the magnetotelluric data such as central impedance (d_3), anisotropy angle (λ) and phase of central impedance (ϕ_{d3}) were prepared with classical magnetotelluric parameters (apparent resistivity and impedance phase), and detailed Mohr-circle displays were shown for selected stations as a function of the Bostick depth. The pseudosections and the Mohr-circle displays suggest that the northeast Thrace region is geologically more complex than the southwest region, where the Istranca Massif bounds the Thrace Basin by a steep NW–SE-oriented fault, possibly with a considerable component of normal slip. In the southwest Thrace region, NE–SW-oriented faults with a component of strike slip occur, forming a broad structural uplift to the north of Saroz Bay. We also find that the most evident changes in geoelectrical strike directions are related to changes in thickness of the upper crust and electromagnetic dimensionality effects, knowledge of which is extremely important in modelling and inversion of data, are predominant on the magnetotelluric data set.

Key Words: Thrace Basin, magnetotellurics, Mohr circles, rotational invariants, anisotropy, geoelectrical strike directions, crust

Türkiye'de Trakya Bölgesi'ndeki Manyetotelurik Verilerin Mohr Dairesi Tabanlı Rotasyonel Sabitleri: Jeolojik Çıkarımlar

Özet: 1995 yazında Avrupa kıtası'nda Kuzeybatı Türkiye'yi güneybatı–kuzeydoğu kesen bir profil boyunca kırk istasyonda manyetotelürik ölçümler alınmıştır. 204 km uzunluğundaki bu hat kuzeydeki metamorfiklerden oluşan Istranca Masifi ile güneyindeki Tersiyer yaşlı bir havza olan Trakya Havzası arasındaki sınırı tanımlamaktadır. Manyetotelürik verisinin Mohr dairesi tabanlı rotasyonel sabit karakteristikleri (merkezcil empedans [d_3], anizotropi açısı [λ], ve merkezcil empedansın fazı [ϕ_{d3}]) ve geleneksel manyetotelürik parametreleri (görünür özdirenç ve empedans fazı) andıran kesitler olarak sunulmuştur. Ayrıca belirli istasyonlar için detaylı Mohr daire gösterimleri, Bostick derinliğinin bir fonksiyonu olarak çizilmiştir. Andıran kesitler ve Mohr dairesi gösterimleri jeolojik olarak havzanın kuzeydoğu kesiminin güneybatıya göre daha karmaşık olduğunu göstermektedir. Kuzeydoğuda Istranca Masifi ile Trakya Havzasını, KB–GD gidişli normal faylar sınırlamaktadır. Trakya Havzasının güneybatısında ise, doğrultu atımlı bileşeni de olan KD–GB doğrultulu faylar Saroz körfezinin kuzeyinde geniş bir yapısal yükselim oluşturmaktadır. Ayrıca jeoelektrik uzanım doğrultularındaki en belirgin değişimlerin üst kabuk kalınlık değişimleri ile ilgili olduğu düşünülmektedir. Manyetotelürik veri grubu üzerinde modelleme ve ters çözüm aşamasında son derece önemli olan elektromanyetik boyutsallık etkilerinin baskın olduğu belirlenmiştir.

Anahtar Sözcükler: Trakya Havzası, manyetotelürik, Mohr daireleri, rotasyonel sabitler, anizotropi, jeoelektrik uzanım doğrultuları, kabuk

Introduction

A variety of rotational invariant techniques is possible to examine magnetotelluric impedance tensors. Many authors have used them to provide information about geoelectric structures (Berdichevsky & Dimitriev 1976; Lilley 1976, 1993a, b, c, 1998a, b; Eggers 1982; Ranganayaki 1984; Spitz 1985; Beamish 1986; LaTorraca *et al.* 1986; Counil *et al.* 1986; Yee & Paulson 1987; Ingham 1988; Groom & Bailey 1989; Park & Liveleybrooks 1989; Fischer & Masero 1994; Szarka & Menvielle 1997).

From among these techniques, we here chose Mohr-circle diagrams. Mohr circles are commonly used for analyzing stress and strain (Passchier 1993), and were first introduced by Lilley (1976), and were developed further by the same researcher (Lilley 1993a, b, c, 1998a, b). The Mohr circle is the preferred graphical representation of an impedance tensor because it is the natural generalization of the simplest representation of a complex-valued vector in a plane; moreover, it enables the display of important information from the impedance tensor concerning the dimensionality of the geoelectric structure and decomposition model parameters (Szarka & Menvielle 1997; Lilley 1998a, b; Makris *et al.* 1999; Bayrak et al 2000; Weaver *et al.* 2000; Balasis & Eftaxias 2003).

Our magnetotelluric data set is from the Thrace region of NW Turkey. Turkey is situated at an important junction in the context of both Mediterranean and world tectonics, where plates are actively colliding and earthquakes occur frequently. In northwestern Turkey, there are two important sedimentary basins. One, the western Black Sea basin, comprises Upper Cretaceous and younger sedimentary strata that reach a thickness of 14 km a top oceanic crust (Finetti *et al.* 1988; Görür & Okay 1996). From the standpoint of petroleum generation, the Thrace Basin (TB) is the other important basin; its infill comprises sedimentary rocks of Middle Eocene to Recent age, the total thickness of which has been estimated to be more than 9 km (Turgut *et al.* 1991; Perinçek 1991). This thick sediment fill covers the important tectonic entities (such as faults, volcanic chimneys and granitic intrusions) and their structural imprints. The Thrace Basin was first explored in the 1950s by the Turkish Petroleum Corporation (TPAO) and several other oil companies, with a view towards developing its hydrocarbon potential. For economic reasons, particular attention in most of the studies was given to stratigraphy, reservoir features, gravity and seismic exploration. In contrast, geoelectromagnetic studies have been limited in the study area. The first magnetotelluric recordings (İlkışık 1980) were made at nine stations along an 80-km, N–S traverse in the Thrace Basin. Bayrak *et al.* (2004) modelled the previously acquired magnetotelluric data set (İlkışık 1980) using two-dimensional (2-D) inverse techniques. However, the rotationally invariant characteristics and dimensionality parameters of the region have not been explored previously. This motivated us to investigate these parameters together with the other classical magnetotelluric parameters of the region.

For this purpose, wide-band magnetotelluric data were acquired at 40 stations along a 204-km, SW–NE transect in the Thrace region in 1995, as part of national marine geological and geophysical investigations in northwestern Turkey. The magnetotelluric profile began in the northeasternmost part of the Thrace region near the Black Sea coast, and ended near Saroz Bay in the southwestern part of the region (Figure 1a). The profile transected the northern Massif, namely the Istranca Massif, and the large Tertiary basin lying to the south, termed the Thrace Sedimentary Basin.

This paper examines the magnetotelluric data set collected in the Istranca Massif and the Thrace Basin from the perspective of geological characteristics and Mohr-circle-based rotational invariant characteristics, such as central impedance (d_3) and anisotropy angle (λ) – the two being good dimensionality indicators – along with phase of central impedance (ϕ_{d3}). Detailed Mohr-circle diagrams (Lilley 1976, 1993a, b, c, 1998a, b) have also been produced and discussed, and pseudosections of the apparent resistivity and phase parameters constructed.

Geological Setting

The Thrace region is located in northwestern Turkey, bordering Bulgaria and Greece, and possesses two major geological features: the Istranca Massif and Thrace Basin. The Istranca Massif is a metamorphic complex, located in the northern part of the region, which underwent metamorphism during the Triassic–Cretaceous and was uplifted prior to the deposition of an Upper Cretaceous volcano-sedimentary association (Yılmaz & Polat 1998; Okay *et al.* 2001). However, some ophiolite and ophiolitic mélange occurs locally in the Rhodope Massif in Greece

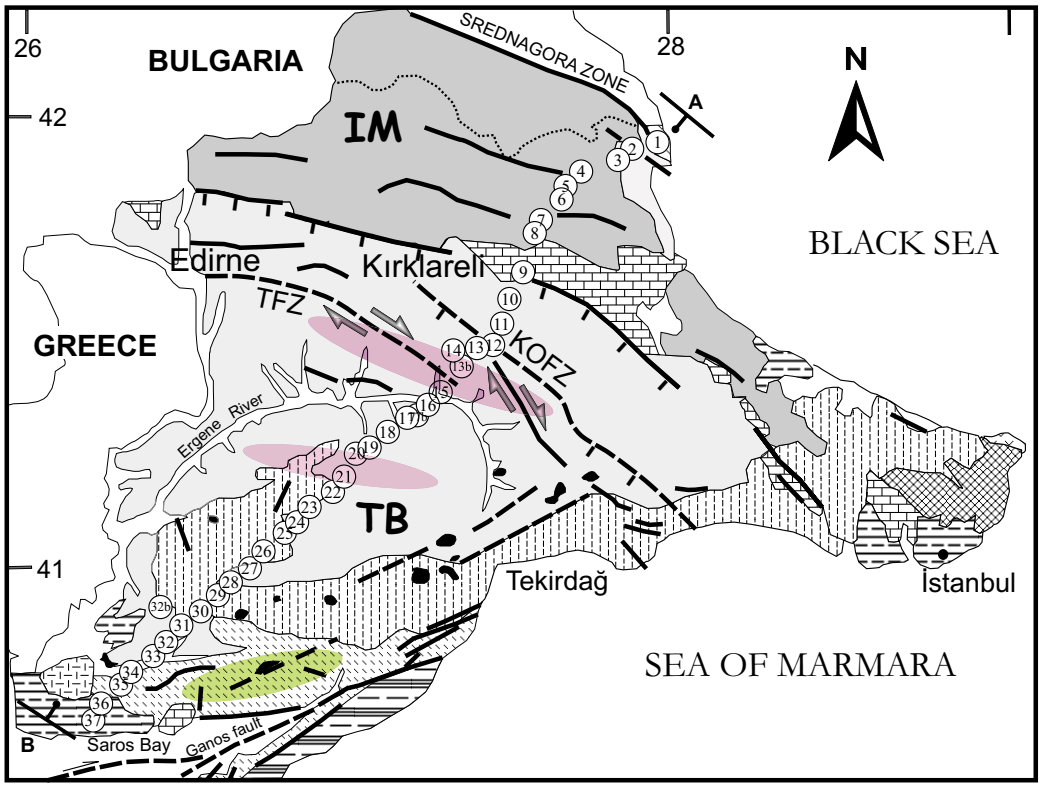

(a)

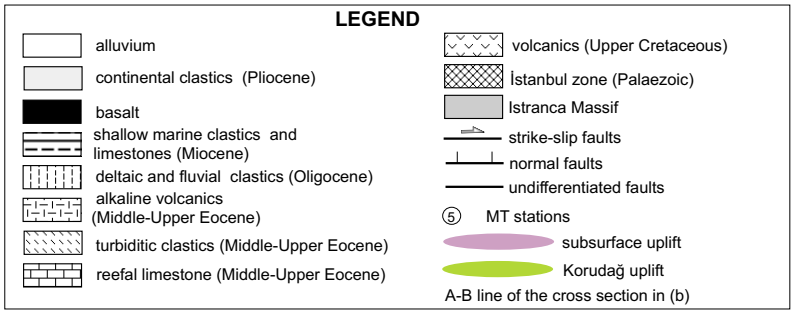

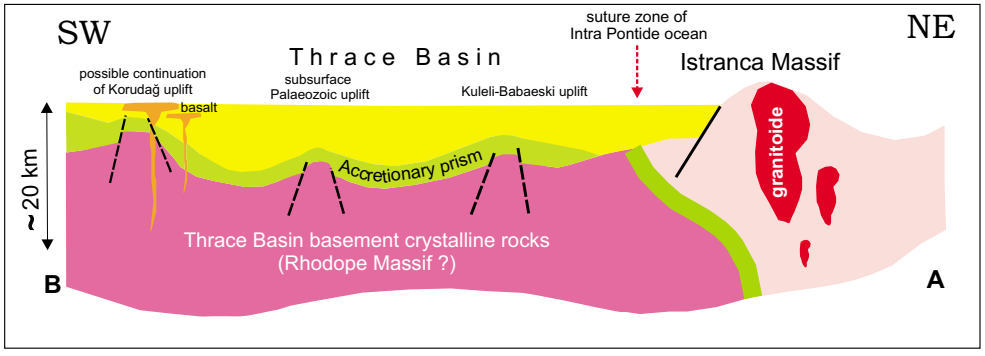

(b)

Figure 1. (a) Simplified geological map of the Thrace region, Turkey. Locations of the 40 magnetotelluric stations are shown by numbers in circles (modified from Görür & Okay 1996; Yılmaz & Polat 1998). (b) Geological cross-section. IM– Istranca Massif, TB– Thrace Basin, TFZ– Terzili Fault Zone, KOFZ– Kuzey Osmancık Fault Zone.

and in the southern part of the Thrace Basin (Beccaletto & Jenny 2004). Şengör & Yılmaz (1981) proposed that the ophiolitic mélange marks the suture of an ocean – the Intra-Pontide Ocean – located between the Istranca Massif to the north and the Sakarya continent to the south.

The Thrace Basin is a large, triangular Tertiary basin, and two major dextral strike-slip fault zones in the basin define this geometry (Perinçek 1991; Turgut *et al.* 1991; Görür & Okay 1996; Yaltırak 2002). It is one of the most important hydrocarbon provinces of Turkey, flanked predominantly by metamorphic rocks of the Istranca Massif to the north. Uplift in the Thrace Basin is apparent at various locations, including the Kuleli-Babaeski uplift in the north, Palaeozoic subsurface uplift in the centre, and the Korudağ uplift (Coşkun 2000) in the south.

Most of our knowledge of the basin structure comes from seismic studies and borehole data (Turgut *et al.* 1991; Perinçek 1991). These studies reveal that the internal structure of the basin consists of numerous folds and faults, trending more-or-less parallel to the basin margins. These faults trend NW–SE in the north and NE–SW in the south, and converge to the east – somewhere in the Sea of Marmara (Görür & Okay 1996).

The northern fault zone is composed of two large subparallel segments, a northern branch and a southern branch, termed the Kuzey Osmancık fault zone and the Terzili fault zone, respectively. These fault zones could only be mapped in the subsurface through drilling and multi-channel reflection seismic data (Turgut *et al.* 1991; Perinçek 1991). The Kuzey Osmancık fault zone is mainly a marginal normal fault with a minor strike-slip component. The NW–SE-trending Terzili fault zone, on the other hand, has deformed the whole of the sedimentary section below the Plio–Quaternary alluvial sedimentary cover in the north-central and northern half of the Thrace Basin, and is no longer active. It is a pure strike-slip fault and affects the whole stratigraphic column, forming flower structures along its path (Turgut *et al.* 1991).

The second fault zone, bordering the southern margin of the basin, is the southwestern strand of the North Anatolian Fault Zone (NAFZ). It has a right-lateral strike-slip fault characteristic, and has caused intense uplift and deformation along the southern margin of the basin. Its deformational influence on the sedimentary record in the southern part of the Thrace Basin suggests a latest Miocene to Early Pliocene age for its development. This fault is still active and causes earthquake activity along the southern shores of the Sea of Marmara. Reverse and thrust faults are abundant in the Ganos region at the southern margin, and in the Çorlu-Terzili belt on the northern margin of the Tharace Basin (Turgut *et al.* 1991; Bozkurt 2001; Westaway 2003; Ekmekçi 2005).

Magnetotelluric Survey and Data Analysis

Magnetotelluric data were acquired in 1995 at 40 stations, using Phoenix V5 multipurpose magnetotelluric instruments, with five base channels (H_X, H_Y, H_Z, E_X, E_Y) and two local remote-reference channels (H_{XR} and H_{YR}). The recording period range was 0.003125–2000 s for all stations. The telluric field variations were measured with typically 100 m bipoles, in a cross-configuration, with non-polarizable Pb-PbCl electrodes. The magnetic fields were measured with coils for the horizontal components and an air loop for the vertical component. The distance between base and remote-reference channels was a few hundred meters, resulting in effective noise cancellation (Gamble *et al.* 1979). The V5 magnetotelluric system is a real-time sounding system. In this system, data acquisition is divided into two frequency ranges. Data in the range 320–7.5 Hz were processed in narrow frequency bands containing two frequencies (the 6^{th} and 8^{th} harmonics of the data-set length). Longer period data, 6–0.0005 Hz, were processed using a cascade decimation scheme (Wight & Bostick 1980).

Mohr-Circle-Based Rotational Invariants

The Mohr-circle diagrams displays relationships between the elements of the impedance tensor, using axes drawn for Z'_{XY} (abscissa) and Z'_{XX} (ordinate), where the dash superscript indicates the value of the appropriate tensor element after the observing axes have been rotated clockwise by angle θ' (Lilley 1993a). All tensor elements are first normalized by multiplication by the square root of period. By such an analysis, it is possible to determine Mohr-circle-based rotational invariants and dimensional characteristics of the geoelectric structures. The parameters for the Mohr-circle presentation of the Z'_{XXr} and Z'_{XYr} impedance tensor elements are defined below (see Figure 2).

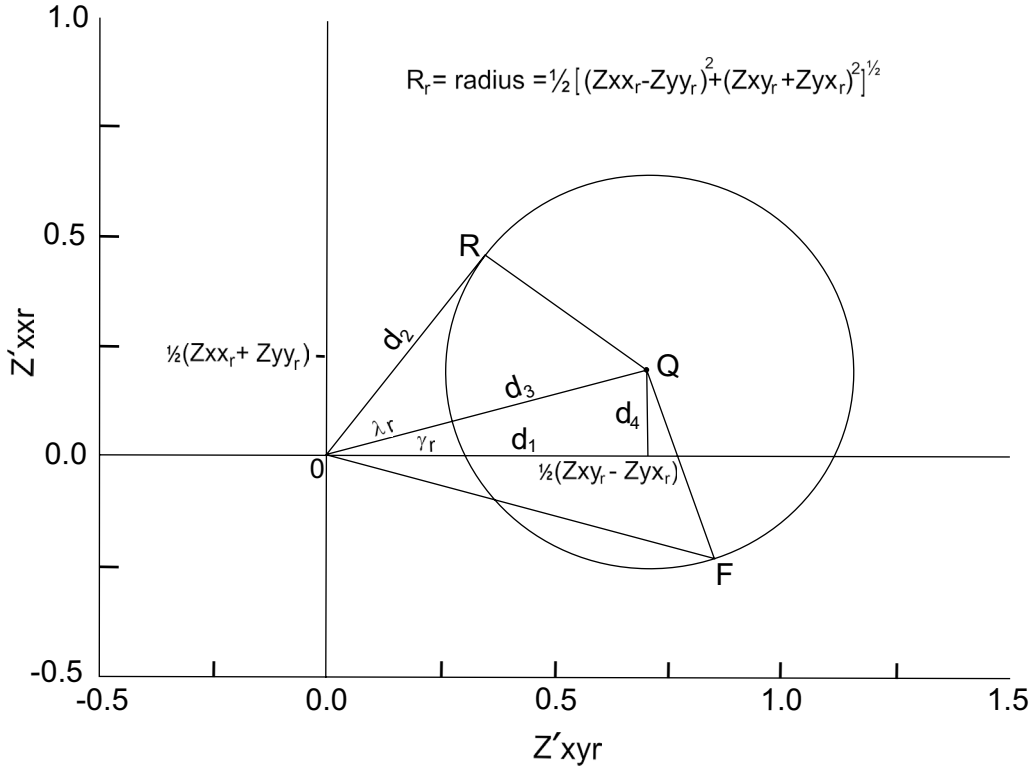

R_r= radius =½[$(Zxx_r-Zyy_r)^2+(Zxy_r+Zyx_r)^2$]^{½}

Figure 2. Mohr representation of the real part of the impedance tensor as a circle. In the figure, d_2 is the magnitude of the determinantal impedance (taking real and imaginary parts separately). d_1 is the second effective (or trace) impedance. The line joining the origin to the center of the circle is the d_3 central impedance which is the basic invariant. λ_r is the anisotropy angle and γ_r is the skew angle. The reference arm is drawn from the circle center to an observed point, such as point F, on the lower right side of the circle (Lilley 1993a; Szarka & Menvielle 1997). A similar diagram can also be drawn for the imaginary part of an impedance tensor.

The centre of the circle is at the point:

$$Z'_{XYr} = \frac{1}{2}(Z_{XYr} - Z_{YXr}) \quad (1a)$$

$$Z'_{XXr} = \frac{1}{2}(Z_{XXr} - Z_{YYr}) \quad (1b)$$

The radius of the circle is given by:

$$R_r = \frac{1}{2}[(Z_{XXr} - Z_{YYr})^2 + (Z_{XYr} + Z_{YXr})^2]^{1/2} \quad (1c)$$

The central impedance is given by:

$$d_{3r} = \frac{1}{2}\left((Z_{XXr} + Z_{YYr})^2 + (Z_{XYr} - Z_{YXr})^2\right)^{1/2} \quad (1d)$$

The anisotropy angle is given by:

$$\lambda_r = \tan^{-1}\left[\frac{\frac{1}{2}\left[(Z_{XXr} - Z_{YYr})^2 + (Z_{XYr} + Z_{YXr})^2\right]^{1/2}}{(Z_{XXr}Z_{YYr} - Z_{XYr}Z_{YXr})^{1/2}}\right] \quad (1e)$$

Where the subscript 'r' denotes the real part of the impedance tensor. Similar expressions apply for the imaginary part of the impedance tensor with subscript 'i'. The radius drawn from the centre of the circle to the originally observed point ($Z_{XYr,i}$, $Z_{XXr,i}$) then forms a radial arm or "reference arm". The orientation of radial arms can be traced for evidence of geologic strike direction (Lilley 1993c). The radial arms of real and imaginary circles are parallel for a 2-D structure and, in the case of

a 3-D structure, may depart from being parallel. These parameters are Mohr-circle-based rotational invariants and independent of the direction of the inducing electromagnetic field and those of the recording axes.

For a tensor with 1-D characteristics, the Mohr circle is simply a point on the $Z'_{XYr,i}$ axis, and the $\lambda_{r,i}$ and $\gamma_{r,i}$ parameters are zero. For a 2-D tensor, the circle has its centre on the $Z'_{XYr,i}$ axis, so that $\lambda_{r,i}$ is nonzero while $\gamma_{r,i}$ is zero. If the tensor, however, shows a 3-D structure, then the circle centre moves off the $Z'_{XYr,i}$ axis; in this case $\lambda_{r,i}$ and $\gamma_{r,i}$ are both nonzero (Figure 2); often such twist increases at low frequency, where the impedance tensor is affected by a larger volume of the earth, so that the likelihood of influences by 3-D structures is increased (Ranganayaki 1984).

In obtaining classical magnetotelluric parameters, it is assumed that the resistivity has a two-dimensional distribution. Then the measuring axes are rotated mathematically until the on-diagonal impedance elements Z_{XX} and Z_{YY} are minimized, while Z_{XY} and Z_{YX} represent the independent transverse magnetic (TM) and transverse electric (TE) modes of polarizations. The TM mode (Figure 3) is defined as having the electric field across-strike direction, while TE mode (Figure 4) has the field parallel to the strike. The TM mode apparent resistivity and impedance phase are derived from the non-diagonal elements of the impedance tensor as a function of frequency as

$$\rho_{XY} = \frac{1}{\omega \mu_0} |Z_{XY}|^2 \qquad (2a)$$

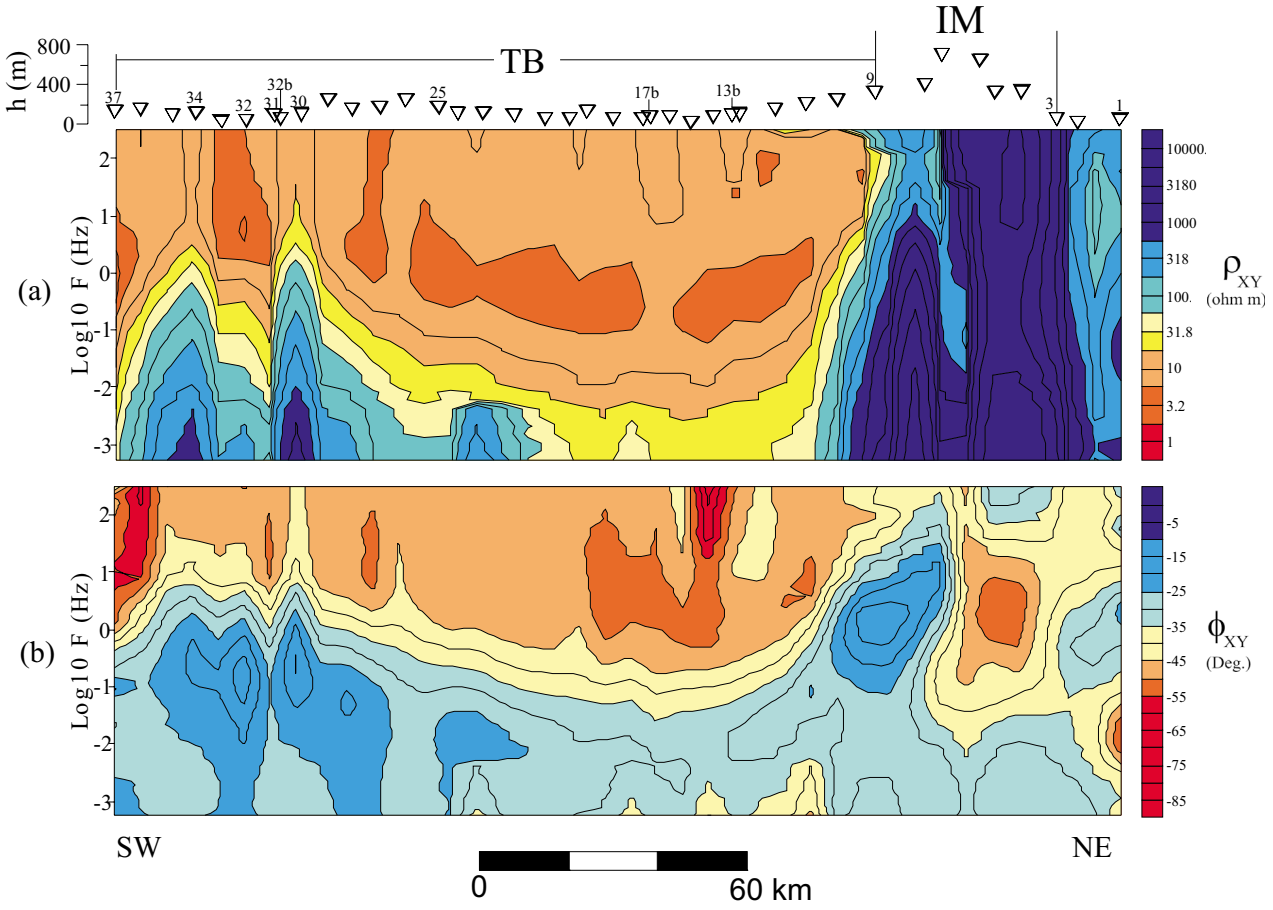

Figure 3. Pseudosections of the TM (ρ_{XY} and ϕ_{XY}) mode data observed along the profile. Contour values of apparent resistivities are in ohm m and phases are in degrees.

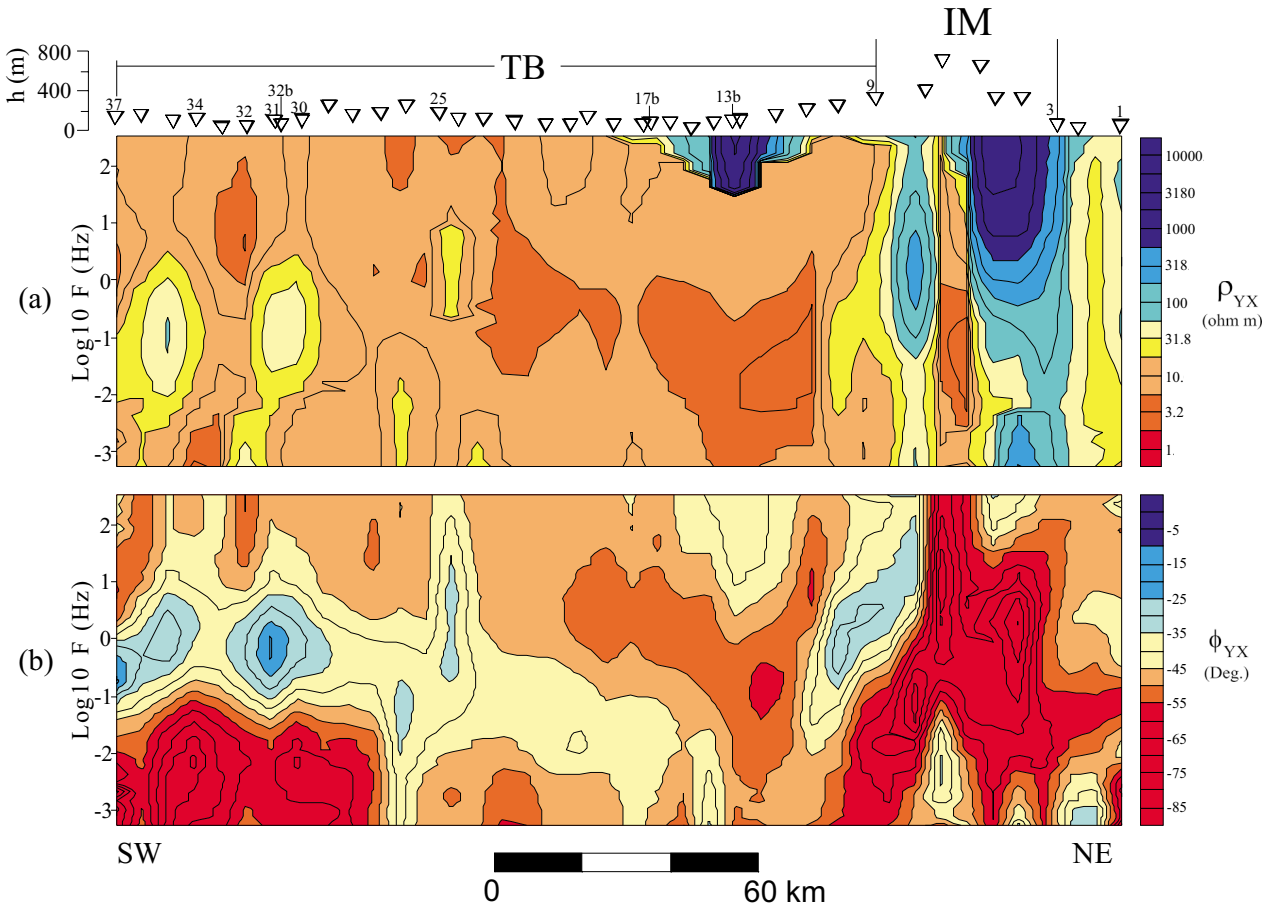

Figure 4. Pseudosections of the TE (ρ_{YX} and ϕ_{YX}) mode data observed along the profile. Construction and labeling are the same as in Figure 3.

and

$$\phi_{XY} = \tan^{-1}\left(\frac{\mathrm{Im}Z_{XY}}{\mathrm{Re}Z_{XY}}\right) \qquad (2b)$$

where $\omega=2\pi f$, μ_0 and f are the magnetic permeability of free space and the frequency in Hz, respectively. Similar expressions apply for the other two-dimensional mode (TE), for ρ_{YX} and ϕ_{YX}.

We have chosen the Bostick (1977) transform to estimate depth and resistivity by using the "central impedance (d_3)" invariant, taking both the real and imaginary parts. Hutton *et al.* (1985) have shown that "invariant" responses can give interface depths closer to the results of 2-D modelling than those obtained from TM and TE mode responses. This transform is used as a starting point for more complicated modelling of the magnetotelluric data, and is used in an attempt to obtain true resistivity versus true depth information. The equation used to calculate the Bostick depth in units of metres is:

$$d_B = 356\left(\frac{\rho_a}{f}\right)^{1/2} \qquad (3a)$$

and Bostick resistivity corresponding to depth d_B

$$\rho_B = \rho_a\,\frac{1-m}{1+m} \qquad (3b)$$

where ρ_a is apparent resistivity computed from "central impedance" in ohm m and "m" is the gradient of the (ρ_a vs f) data on a logarithmic scale.

Results and Discussion

The pseudosections of Mohr-circle-based rotational invariant characteristics (d_3 and λ) and phase of central impedance (ϕ_{d3}) have been constructed together with the traditional magnetotelluric parameters of apparent resistivity and impedance phase. Also, detailed Mohr circles displayed as a function of the Bostick depth are shown for selected stations. Thus, Figure 3 shows pseudosections of TM mode apparent resistivity (ρ_{XY}, ohm m) and phase (ϕ_{XY}, degree) of the off-diagonal elements observed along the profile. Between stations 37–9, conductive features (<17.5 ohm m) are noted in the ρ_{XY} pseudosection and low phase values (< -45° down to –90°) are noted in the ϕ_{XY} pseudosection. Between stations 9 and 3, high resistivity values are apparent in the ρ_{XY} pseudosection. At station 7, a phase contrast is rather clear in the ϕ_{XY} pseudosection. Figure 4 shows pseudosections of the TE mode apparent resistivity (ρ_{YX}, ohm m) and phase (ϕ_{YX}, degree) of the off-diagonal elements observed along the profile. In the ρ_{YX} pseudosection between stations 37–9, conductive features are apparent at all frequencies. In the ϕ_{XY} pseudosection, high negative phase values are predominant. Similar to the TM mode results near station 7, a phase contrast is noticeable in the ϕ_{XY} pseudosection.

Figure 5 shows pseudosections of the central impedances (d_3), determined for both the real and imaginary parts of the impedance tensors. Previous work suggests that the central impedance (d_3) parameter is a good indicator of main geological structure because anomalies are more evident and less complicated (e.g., Bayrak *et al.* 2000). Both in the real and imaginary

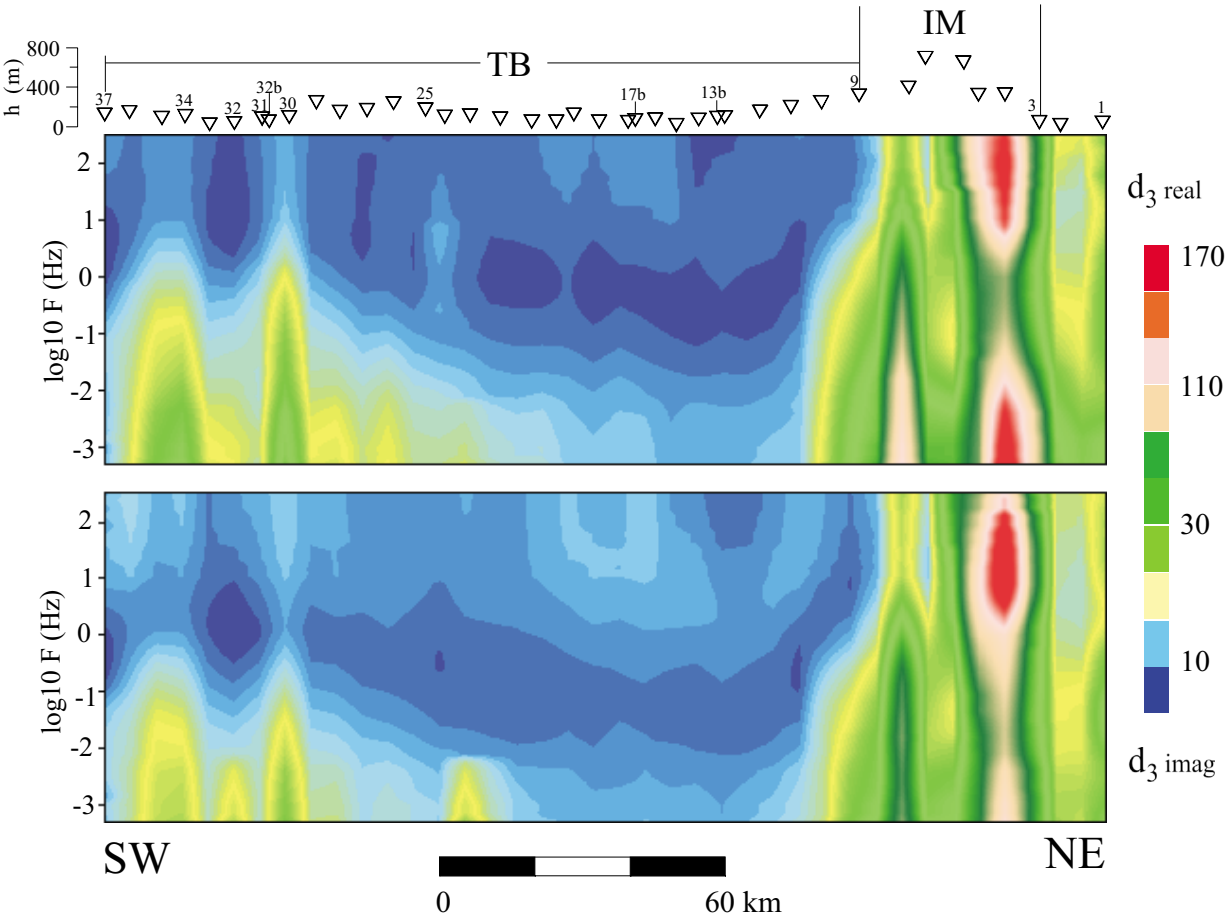

Figure 5. Pseudosections of central impedance (d_3) for the profile, drawn for the real and imaginary parts of the impedance tensors, respectively. The unit is that of normalized impedance, described in the text.

pseudosections, blue-colour values of about 10 occur from the SW to station 9. Between stations 36–28 central impedance values reach to ~20 below the frequency of 1 Hz. Central impedance has values greater than 20 between stations 9 and 1. Between stations 5 and 4, central impedance acquires very large values in the range of 320–1 Hz and 0.01–0.0005 Hz.

Figure 6 shows pseudosections of the anisotropy angle values (λ, degrees), determined for both the real and imaginary parts of the impedance tensors. In the real and imaginary pseudosections, blue tones – corresponding to anisotropy angles of about 10° – occur between stations 37–8, and anisotropy angles of more than 30° between stations 8–3. Similar to the central impedance, in the SW part of the profile, between stations 36–28, anisotropy values exceed ~30° at lower frequency bands. At station 7, very high anisotropy angle values (>60°), spreading with depth, are noticeable at almost all frequencies, in both the real and imaginary pseudosections.

Figure 7 shows the phase angle plotted versus Bostick (1977) depth. Central impedances were used to compute both phase angles and Bostick depths. Ranganayaki (1984) has shown that the phase angle of the "invariant" impedances is particularly sensitive to lateral and vertical variations in crustal resistivity and may be used in pseudosection form to delineate qualitatively the conductive and resistive zones. High phase values indicate sounding from relatively resistive to relatively conductive materials. Thus, the computed phase values show

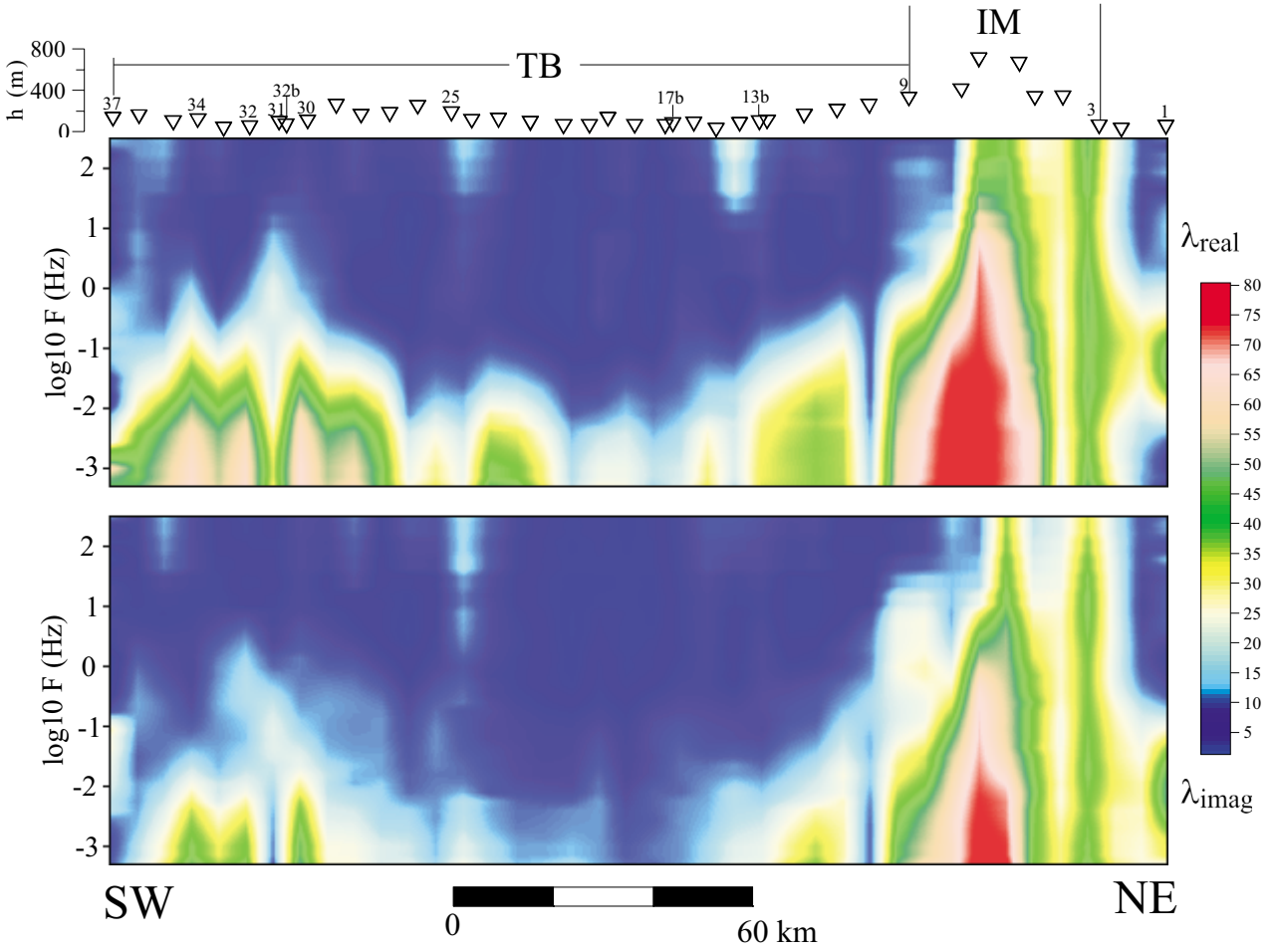

Figure 6. Pseudosections of anisotropy angle (λ, degrees) for the profile, drawn for the real and imaginary parts of the impedance tensors, respectively.

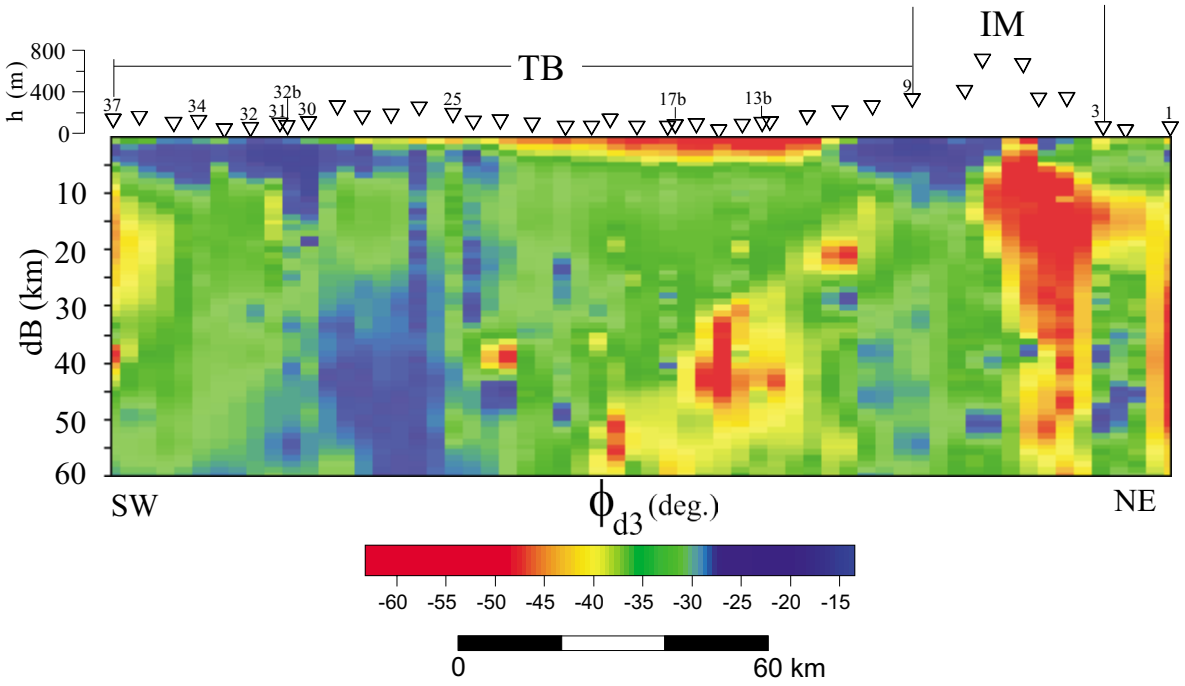

Figure 7. Phase pseudosection calculated from the "central impedance". Red indicates phases below 45° – a transition from conductive to resistive structures with increasing depth. Vertical scale is "penetration depth", after Bostick (1977). Horizontal scale is distance in kilometers.

themselves very clearly, with high values in the Thrace Basin and Istranca Massif structures. Meanwhile, high phase values between stations 19–11 beneath the Thrace Basin (at a depth of ~20–55 km) point out a probable change of resistive-conductive structure. The pseudosection of phase of central impedance compares well with the geological cross-section along the magnetotelluric profile (Figure 1b). This parameter might be useful in obtaining actual structural features of the area and would be extremely useful in quantitative modelling (Ranganayaki 1984).

The Bostick resistivity inversion pseudosection for a depth of 60 km along the profile is given in Figure 8. The resistivity values, which are smaller than 30 ohm m and continue to a maximum depth of 10 km, indicate sediments of the Tharace Basin at stations between 37–9 in the Bostick pseudosection. The maximum thickness of sediments in the Thrace Basin has been found to be ~ 9 km in several studies (Turgut *et al.* 1991; Perinçek 1991; Görür & Okay 1996). The Thrace Basin is located near several other basins; namely, the Black Sea basin located to the northeast, the Sea of Marmara basin to the south and southeast, and the Aegean Sea basin to the southwest (Figure 1a). In western and northwestern Turkey, the thicknesses of sedimentary units are between 1 and 8 km, according to the 2-D magnetotelluric studies of Bayrak & Nalbant (2001), Çağlar (2001), Gürer (1996), Gürer *et al.* (2001, 2002, 2004a, b), Tank *et al.* (2003) and Bayrak *et al.* (2004). High resistivity values (>700 ohm m) continuing to deeper parts represent the Istranca Massif crystalline basement rocks at the stations between 9–3. The presence of a layer relatively conductive (~80 ohm m) and located at depths of 12–25 km is seen beneath the TB (Bayrak *et al.* 2004). The two-dimensional georesistivity model of another magnetotelluric data set in the region (Bayrak *et al.* 2004) indicates that this structure is an undulating ~10-km-thick layer, interpreted as a conductive part of the lower crust. A structure with 400 ohm m resistivity is present at the base of the sedimentary fill of the Thrace Basin (in the model of Bayrak *et al.* 2004). This structure is not homogeneous but rather includes scattered blocks with Istranca Massif resistivity (>700 ohm m). According to Yılmaz (1995), a gravity modelling study has shown that, beneath the sediments of the Thrace Basin, there is no calm environment. Seismic lines run in 1993 and 1994 also support these results (Coşkun 2000). Several faults are present within the Thrace Basin, such as the Terzili fault zone and Kuzey Osmancık fault zone, crossing it in

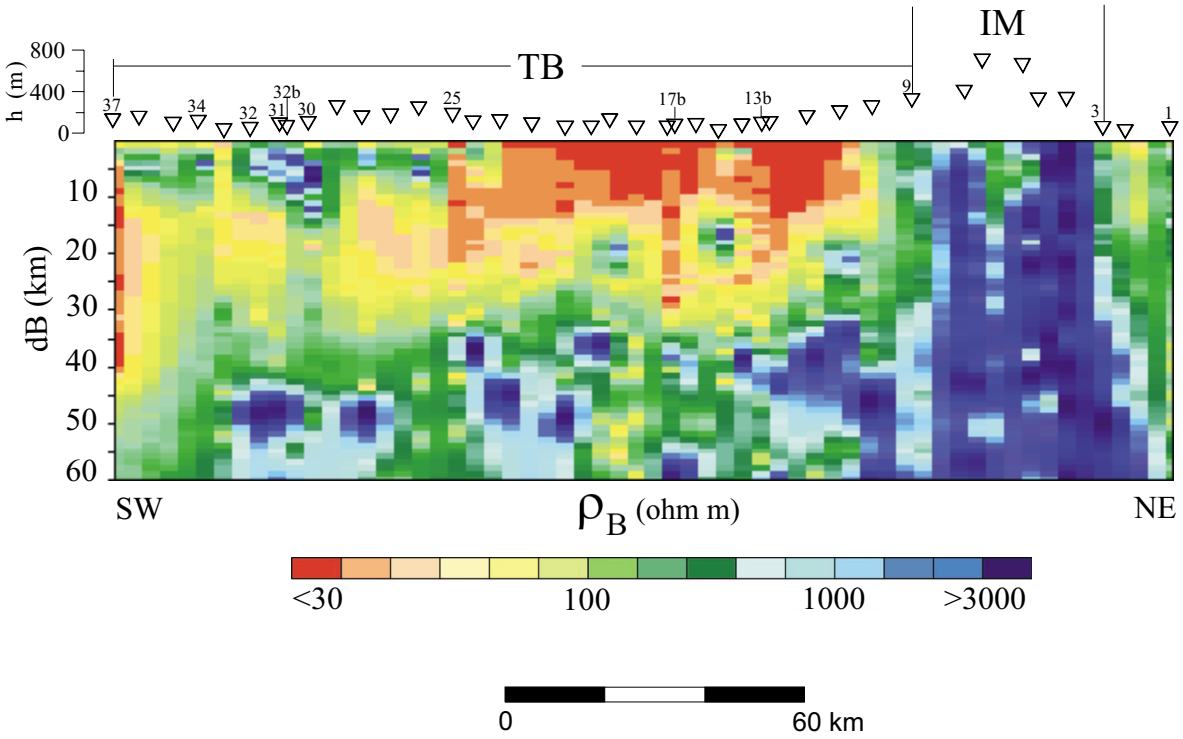

Figure 8. Bostick resistivity pseudosections along the profile. Station locations along the horizontal axis and depths (km) on the vertical axis.

a NW–SE direction. The structure between stations 25 and 9 arises from the geometry of the Terzili fault zone and Kuzey Osmancık fault zone.

Figure 9 shows detailed Mohr-circle diagrams results for eight characteristic stations (stations 36, 34, 30, 28, 12, 7, 3 and 1, from southwest to northeast) for 20 frequencies, together with equivalent Bostick (1977) depths. Bostick depths were computed by using central impedances. Real circles are located above in the figure, imaginary circles below. Station 36 is located on the shallow-marine clastics, and real circles show 1-D structural characteristics down to about 8-km depth. At this depth, 2-D structural characteristics and strong anisotropy are predominant on the real circles while strike directions are changing. Station 34 is located on turbiditic clastics. For this station, circles have 1-D structure down to 1.5-km depth in real section. At this depth, to a depth of about 12 km, 2-D structures are influential. At greater depths, effects of 3-D structure – such as anisotropy and skew – are clearly predominant. Also, strike changes its direction beginning at about 4-km depth in the real section. In the imaginary section down to 17-km depth, circles show 1-D characteristics while greater depths show 3-D structures with changes of strike direction. When the geology is more complicated, as seen in this station, the real and imaginary circles may well start to vary from one another. Station 30 is located on deltaic and fluvial clastics and, in the real section – down to 2-km depth – 1-D structure is predominant. At 3.5 km and greater depths, increasing anisotropy and excellent 2-D structure is present. Another important feature of this section is a change in strike at about 20-km depth. In the imaginary section, 2-D structure is present from this depth. The radial arms of real and imaginary circles are also parallel around these depths, indicative of 2-D geology. Station 28 is located on continental clastics. For this station, 1-D structure extends down to about 2 km in the real section. At this depth, circles show 2-D characteristics with strong anisotropy values, while strike begins to change its direction.

Pseudosections of invariants and Mohr-circle diagrams, in the southwestern part of the Thrace Basin, show 2-D geoelectric structural characteristics, strong

Figure 9. Mohr circles drawn for the real (above) and imaginary (below) parts of the impedance tensors, for stations 36, 34, 30, 28, 12, 7, 3 and 1, from southwest to northeast along the profile. The radial arm or "reference arm" is indicated for each Mohr circle. Bostick depths (in km) for each frequency are shown in a column with heading dB (km) column. These depths also apply to the respective imaginary figures, given below. The scale of the figure for real and imaginary axes is shown at the bottom of the imaginary sections.

anisotropy, and high central impedance values below a frequency of ~1 Hz. These anomalies may be related to the numerous outcrops of basaltic and andesitic eruptive centres in the southwestern part of the Thrace Basin (Figure 1b).

Station 12 is located on the Thrace Basin and Kuzey Osmancık fault zone, the latter mapped by seismic studies (Turgut *et al.* 1991; Perinçek 1991). In the real section, 1-D structure is noted down to a 1.3-km depth, whilst at depths between 1.3 and 26 km, moderate anisotropy and 2-D characteristics are noted and, at greater depths, 3-D structures.

Station 7 is located on the Istranca Massif. In the real section at greater depths from the surface, increasing anisotropy and 3-D structures are observed. At about 15-km depth, a change in strike is notable and, where the circles go near (even through) the origin, very high anisotropy of the impedance tensor is indicated. Departure of the radial arms of real and imaginary circles from being parallel indicates 3-D geology. Station 3 is near station 7 and located on continental clastics. Similar to station 7, 3-D structures and very strong anisotropy are quite evident at all frequencies. In particular, the presence of very strong anisotropy, which increases from 10-km depth and downward, is seen. Furthermore, strike has a different orientation at this depth. Such consistency between stations that are near each other implies regional two-dimensional and three-dimensional structural effects, knowledge of which may be important in modelling the data (Lilley 1993b). The Istranca Massif collides with the Srednogorie zone farther north along a reverse fault dipping to the south (Figure 1). Very strong anisotropy values may characterize this reverse fault/collision event at 10-km depth (Okay *et al.* 2001). Station 1 is located on the Istranca Massif, and in the real section, all circles have 3-D structure. The most prominent, strongest anomaly is at about 30-km depth, with highest anisotropy and changing strike direction. From this depth on, anisotropy dramatically decreases.

Rotational invariants and Mohr-circle diagrams anomalies with strong 3-D effects, high anisotropy and phase angles (at the NE end of the profile) show that the Istranca Massif – manifested via high resistivity values (700 ohm m or higher) – is not homogeneous. These anomalies, in the northeastern part of the profile, may be correlated to the several outcrops of Late Cretaceous granitic intrusions within the Istranca Massif (Figure 1b). According to Okay *et al.* (2001), the Istranca Massif is a composite orogenic belt deformed and regionally metamorphosed during Late Variscan and Late Jurassic–Early Cretaceous orogenesis.

The most evident changes in geoelectrical strike directions are observed at Bostick depths of ~8, 4, 20, 15 and 30 km along the profile from southwest to northeast, and may be related to changes in thickness of the upper crust, as indicated by previous studies (Meissner *et al.* 1987; Novotny *et al.* 2001; Van der Meijde *et al.* 2003; Bayrak *et al.* 2004). Moreover, these changes may be related to facies changes in sediments (in 4 to 8 km depths) and/or to variations in crystallinity in the basement rocks (at 15, 20, 30 km depths) (e.g., see Bayrak *et al.* 2000).

Conclusion

Magnetotelluric surveys in the Thrace region of Turkey, conducted in 1995, included 40 sites located in the Thrace Basin and Istranca Massif. We have studied Mohr-circle-based rotational invariants, such as central impedance, anisotropy angle, phase of central impedance and Mohr-circle diagrams, and correlated these parameters by means of Bostick inversion. The results of these parameters of the magnetotelluric data set have provided some major findings:

1. Pseudosections of Mohr-circle-based rotational invariants, Mohr-circle diagrams and Bostick inversion clearly show the main geoelectric structures of the Thrace region along the profile. The Thrace Basin extends for about 150 km SW–NE between stations 37 and 9, and consists of poorly-consolidated sediments (resistivity ~30 ohm m or less) to a depth of about 10 km in its centre and ~1 km in its southwestern part. Below the Thrace Basin, the presence of a relatively conductive layer (~80 ohm m), reaching depths of between 12–25 km, is observed. This layer may correlate to the seismic reflector which results from density differences within the metamorphic units in the crystalline basement rocks of the upper crust (Yılmaz 1995). The Bostick resistivity inversion pseudosection indicates a complex geological setting for the southwestern Thrace Basin. The resistive crystalline rocks seem to occur nearer the surface in the southwestern part of the Thrace Basin than in the northeastern and central parts of the basin, as manifested by Palaeozoic exposures at the southwestern margin of Thrace Basin. These features cause the Thrace Basin to

have the shape of an asymmetrical "W" between stations 25 and 9 along the profile, and may be related to numerous outcrops of a basaltic eruptive centre in the southwestern part of the TB (Aldanmaz *et al.* 2005, 2006) (Figure 1b).

2. The detailed Mohr-circle display shows that the circles have perfect 1-D structural features in the Thrace Basin, while they show rather complicated strong anisotropy, skew and changing strike direction beneath the Thrace Basin. Also, Mohr circles on the Istranca Massif show strong anisotropy, skew, electromagnetic dimensionality effects and changing strike directions from the surface to depth. These results support the finding that the Istranca Massif, at the NE end of the profile, is not homogeneous and may comprise several different crystalline phases, such as granititic intrusions (Okay *et al.* 2001; Gerdjikov 2005), andesites, peridodites and serpentines, et cetera within the Istranca Massif (Figure 1b).

3. The phase of central impedance compares well with the extent of the Thrace Basin and Istranca Massif. Similarly, low and high phase zones correlate well with the structures of the volcanic eruptive centres in the southwestern part, and granitic intrusions in northeastern part of the Thrace Basin. Also, high negative phase values beneath the Thrace Basin correlate well with scattered highly resistive crystalline blocks in the basement. We show that the phase parameter may be helpful in obtaining actual rock characteristics of the study area.

4. The most evident changes in geoelectrical strike directions are attributed to changes in thicknesses of the upper crust along the profile.

5. Finally, the results of this paper indicate that Mohr-circle-based rotational invariant parameters – knowledge of which are extremely important in modelling and inversion of magnetotelluric data – will provide guidance to further research aimed at 2-D modelling and inversion of the present data set.

Acknowledgements

The Research Fund of İstanbul University, under Project Numbers 1547/16012001 and BYP-401/26042004 that was directed by the first author, supported this work. This work was also supported in part by TÜBİTAK grant YDABCAG-230/G project (coordinated by Naci Görür); only publication of the rotational invariants of the magnetotelluric dataset was allowed. The authors are indebted to Professor Erdin Bozkurt for his detailed review of the paper that contributed much to its present form. The authors wish to thank Dr. F.E.M (Ted) Lilley, Dr. Laszlo Szarka and Dr. Süleyman Turgut for their contributions to and improvement of the manuscript. We also thank Cemal Kaya, Tuğrul Tokgöz and George Elliot for their efforts to obtain a high-quality magnetotelluric dataset. We are also grateful to Joanna Read for her assistance in improving our English exposition.

References

ALDANMAZ, E., GOURGAUD, A. & KAYMAKÇI, N. 2005. Constraints on the composition and thermal structure of the upper mantle beneath NW Turkey: evidence from mantle xenoliths and alkali primary melts. *Journal of Geodynamics* **39**, 277–316.

ALDANMAZ, E, KÖPRÜBAŞI, N., GÜRER, Ö.F., KAYMAKÇI, N. & GOURGAUD, A. 2006. Geochemical constraints on the Cenozoic, OIB-type alkaline volcanic rocks of NW Turkey: implications for mantle sources and melting processes. *Lithos* **86**, 50–76.

BALASIS, G. & EFTAXIAS, K. 2003. Inversion and modelling of the Ioannina electromagnetic response data. *Geophysical Research Abstracts, European Geophysical Society* **5**, p. 426.

BAYRAK, M., İLKIŞIK, O.M., KAYA, C., & BAŞOKUR, A.T. 2000. Magnetotelluric data in western Turkey: dimensionality analysis using Mohr circles. *Journal of Geophysical Research* **105**, 23391–23401.

BAYRAK, M. & NALBANT, S.S. 2001. Conductive crust imaged in western Turkey by MT. *Geophysical Research Letters* **28**, 3521–3524.

BAYRAK, M., GÜRER, A. & GÜRER, Ö.F. 2004. Electromagnetic imaging of the Thrace Basin and Intra-Pontide Subduction Zone, northwestern Turkey. *International Geology Review* **46**, 64–74.

BEAMISH, D. 1986. Geoelectrical structural dimensions from magnetotelluric data: methods of estimation, old and new. *Geophysics* **51**, 1298–1309.

BECCALETTO, L & JENNY, C. 2004. Geology and correlation of the Ezine Zone: a Rhodope fragment in NW Turkey? *Turkish Journal of Earth Sciences* **13**, 145–176.

BERDICHEVSKY, M.N. & DMITRIEV, V.I. 1976. Basic principles of interpretation of magnetotelluric curves. *In*: ÁDAM, A. (ed), *Geoelectric and Geothermal Studies*. KAPG Geophysical Monograph, Akademiai Kaido, Budapest, 165–221.

BOSTICK, F.X. 1977. A simple almost exact method of MT analysis. *Workshop on Electrical Methods in Geothermal Exploration*. U.S. Geological Survey, Contract no. 14080001-8–359.

BOZKURT, E. 2001. Neotectonics of Turkey: a synthesis. *Geodinamica Acta* **14**, 3–30.

COUNIL, J.L., LEMOUEL, J.L. & MENVIELLE, M. 1986. Associate and conjugate direction concepts in magnetotellurics. *Annales Geophysicae* **B4**, 115–130.

COŞKUN, B. 2000. Influence of the Istranca-Rhodope Massifs and strands of the North Anatolian Fault on oil potential of Thrace Basin, NW Turkey. *Journal of Petroleum Science and Engineering* **27**, 1–25.

ÇAĞLAR, İ. 2001. Electrical resistivity structure of northwestern Anatolia and its tectonic implications for the Sakarya and Bornova zones. *Physics of the Earth and Planetary Interiors* **28**, 95–110.

EGGERS, D.E. 1982. An eigenstate formulation on the magnetotelluric impedance tensor. *Geophysics* **47**, 1204–1214.

EKMEKÇİ, M. 2005. Karst in Turkish Thrace: compatibility between geological history and karst type. *Turkish Journal of Earth Sciences* **14**, 73–90.

FINETTI, I., BRICCHI, G., DEL BEN, A., PIPAN, M. & XUAN, Z. 1988. Geophysical study of the Black Sea. *Bolletino di Geofisica Teorica ed Applicata, Monograph on the Black Sea,* **30**/117–118:197–324.

FISCHER, G. & MASERO, W. 1994. Rotational properties of the magnetotelluric impedance tensor: the example of the Araguainha impact crater, Brazil. *Geophysical Journal International* **119**, 548–560.

GAMBLE, T.D., GOUBAU, W.M. & CLARKE, J. 1979. Magnetotellurics with a remote magnetic reference. *Geophysics* **44**, 53–68.

GERDJIKOV, I. 2005. Alpine metamorphism and granitoid magmatism in the Strandja Zone: new data from the Sakar Unit, SE Bulgaria. *Turkish Journal of Earth Sciences* **14**, 167–183.

GÖRÜR, N. & OKAY, A.İ. 1996. A fore-arc origin for the Thrace Basin, NW Turkey. *Geologische Rundschau* **85**, 662–668.

GROOM, R.W. & BAILEY, R.C. 1989. Decomposition of magnetotelluric impedance tensors in the presence of local three-dimensional galvanic distortion. *Journal of Geophysical Research* **94**, 1913–1925.

GÜRER, A. 1996. Deep conductivity structure of the North Anatolian Fault Zone and the İstanbul and Sakarya Zones along the Gölpazarı-Akçaova profile, northwest Anatolia. *International Geology Review* **38**, 727–736.

GÜRER, A., GÜRER, Ö.F., PINÇE, A. & İLKIŞIK, O.M. 2001. Conductivity structure along the Gediz graben, west Anatolia, Turkey: Tectonic implications. *International Geology Review* **43**, 1129–1144.

GÜRER, A., PINÇE, A., GÜRER, Ö.F. & İLKIŞIK, O.M. 2002. Resistivity distribution in the Gediz graben and its implications for crustal structure. *Turkish Journal of Earth Science* **10**, 15–25.

GÜRER, A., BAYRAK, M. & GÜRER, Ö.F. 2004a. Magnetotelluric images of the crust and mantle in the southwestern Taurides, Turkey. *Tectonophysics* **391**, 109–120.

GÜRER, A., BAYRAK, M., GÜRER, Ö.F. & İLKIŞIK O.M. 2004b. The deep resistivity structure of southwestern Turkey: tectonic implications. *International Geology Review* **7**, 655–670.

İLKIŞIK, O.M. 1980. *Trakya'da Yerkabuğunun Manyetotelurik Yöntemle İncelenmesi [Magnetotelluric Study of Continental Crust in Thrace].* Ph.D. Thesis, İstanbul Technical University [unpublished, in Turkish with English abstract].

INGHAM, M.R. 1988. The use of invariant impedances in magnetotelluric interpretation; *Geophysical Journal* **92**, 165–169.

HUTTON, V.R.S., DAWES, G.J.K., DEVLIN, T. & ROBERTS, R. 1985. A broadband tensorial magnetotelluric study in the Travale-Radicondoli geothermal field. *Geothermics* **14**, 645–652.

LATORRACA, G.A., MADDEN, T.R. & KORRINGA, J. 1986. An analysis of the magnetotelluric impedance for three-dimensional conductivity structures. *Geophysics* **51**, 1819–1829.

LILLEY, F.E.M. 1976. Diagrams for magnetotelluric data. *Geophysics* **41**, 766–770.

LILLEY, F.E.M. 1993a. Magnetotelluric analysis using Mohr circles. *Geophysics* **58**, 1498–1506.

LILLEY, F.E.M. 1993b. Mohr circles in magnetotelluric interpretation (i) simple static shift; (ii) Bahr's analysis. *Journal of Geomagnetism and Geoelectricity* **45**, 833–839.

LILLEY, F.E.M. 1993c. Three-dimensionality of the BC87 magnetotelluric data set studied using Mohr circles. *Journal of Geomagnetism and Geoelectricity* **45**, 1107–1113.

LILLEY, F.E.M. 1998a. Magnetotelluric tensor decomposition: 1. Theory for a basic procedure. *Geophysics* **63**, 1885–1897.

LILLEY, F.E.M. 1998b. Magnetotelluric tensor decomposition: 2. Examples of a basic procedure. *Geophysics* **63**, 1898–1907.

MAKRIS, J., BOGRIS, N. & EFTAXIAS, K. 1999. A new approach in the determination of characteristic directions of the geoelectric structure using Mohr circles. *Earth Planets and Space* **51**, 1059–1065.

MEISSNER, R., WEVER, T. & FLÜH, E. 1987. The Moho in Europe - implications for crustal development. *Annales Geophysicae* **5B**, 357–364.

NOVOTNY, O., ZAHRADNIK, J. & TSELENTIS, G.A. 2001. Northwestern Turkey earthquakes and the crustal structure inferred from surface waves observed in the Corinth Gulf, Greece. *Bulletin of the Seismological Society of America* **91**, 875–879

OKAY, A.İ., SATIR, M., TÜYSÜZ, O., AKYÜZ, S. & CHEN, F. 2001. The tectonics of the Strandja Massif: Late-Variscan and mid-Mesozoic deformation and metamorphism in the northern Aegean. *International Journal of Earth Sciences* **90**, 217–233.

PARK, S.K. & LIVELYBROOKS, D.W. 1989. Quantitative interpretation of rotationally invariant parameters in magnetotellurics. *Geophysics* **54**, 1483–1490.

PASSCHIER, C.W. 1993. The sliding-scale Mohr diagram. *Tectonophysics* **218**, 367–373.

PERİNÇEK, D. 1991. Possible strand of the North Anatolian fault in the Thrace Basin, Turkey: an interpretation. *American Association of Petroleum Geologists Bulletin* **75**, 241–257.

RANGANAYAKI, R.P. 1984. An interpretive analysis of magnetotelluric data. *Geophysics* **49**, 1730–1748.

SPITZ, S. 1985. The magnetotelluric impedance tensor properties with respect to rotation. *Geophysics* **50**, 1610–1617.

SZARKA, L. & MENVIELLE, M. 1997. Analysis of rotational invariants of the magnetotelluric impedance tensor. *Geophysical Journal International* **129**, 133–142.

ŞENGÖR, A.M.C. & YILMAZ, Y. 1981. Tethyan evolution of Turkey: a plate tectonic approach. *Tectonophysics* **75**, 181–241.

TANK, S.B., HONKURA, Y., OGAWA, Y., OSHIMAN, N., TUNÇER, M.K., MATSUSHIMA, M., ÇELIK, C., TOLAK, E. & IŞIKARA, A.M. 2003. Resistivity structure in the western part of the fault rupture zone associated with the 1999 İzmit earthquake and its seismogenic implication. *Earth Planets and Space* **55**, 437–442.

TURGUT, S., TÜRKASLAN, M. & PERİNÇEK, D. 1991. Evolution of the Thrace sedimentary basin and hydrocarbon prospectivity. *In*: SPENCER, A.M. (ed), *Generation, Accumulation and Production of Europe's Hydrocarbons*. Special Publication of the European Association of Petroleum Geoscientists, Oxford University Press, Oxford, 415–437.

VAN DER MEIJDE, M., VAN DER LEE, S. & GIARDINI, D. 2003. Crustal structure beneath broad-band seismic stations in the Mediterranean region. *Geophysical Journal International* **152**, 729–739.

WEAVER, J.T., AGARWAL, A.K. & LILLEY, F.E.M. 2000. Characterization of the magnetotelluric tensor in terms of its invariants. *Geophysical Journal International* **141**, 321–336.

WESTAWAY, R. 2003. Kinematics of the Middle East and Eastern Mediterranean updated. *Turkish Journal of Earth Sciences* **12**, 5–46.

WIGHT, D.E. & BOSTICK, F.X. 1980. Cascade decimation-a technique for real time estimation of power spectra. *Institute of Electrical and Electronics Engineers (IEEE) International Confeference, Accoustic, Speech and Signal,* Proceedings 626–629.

YEE, E. & PAULSON, K.V. 1987. The canonical decomposition and its relationship to other forms of magnetotelluric impedance tensor analysis. *Geophysical Journal* **61**, 173–189.

YALTIRAK, C. 2002. Tectonic evolution of the Marmara Sea and its surroundings. *Marine Geology* **190**, 493–529.

YILMAZ, A. 1995. Gravity-magnetic modelling of Thrace Basin and Istranca area. *Symposium on the Geology of the Thrace Basin*, Lüleburgaz-Kırklareli, Turkey. Türkiye Petrolleri A.O. Genel Müdürlüğü, Ankara, Türkiye, 19–20.

YILMAZ, Y. & POLAT, A. 1998. Geology and evolution of the Thrace volcanism, Turkey. *Acta Vulcanologica* **10**, 293–303.

Received 20 February 2005; revised typescript accepted 25 November 2005